Materials Advances

PAPER

View Article Online
View Journal | View Issue

Check for updates

Cite this: *Mater. Adv.*, 2025, **6**, 8131

Received 23rd August 2025,
Accepted 19th September 2025

DOI: 10.1039/d5ma00947b

rsc.li/materials-advances

A study on the third-order nonlinear optical properties of pure $KMnO_4$ using the CW Z-scan technique

R. Santhosh Kumar, * Eldo Abraham Thomas and Sandeep Suresh

Potassium permanganate ($KMnO_4$) is a remarkably versatile compound with a wide range of applications spanning from household to industrial settings. As a neutral salt, it possesses potent oxidizing properties that make it indispensable in various fields. The third-order nonlinear optical properties of pure $KMnO_4$ solution with different normality of 0.05 N, 0.0166 N, 0.0125 N, and 0.009 N have been studied using the Z-scan technique with a continuous wave diode pumped solid state (DPSS) 532 nm laser source of 100 mW. By evaluating the closed aperture and the open aperture response, the nonlinear refractive index (n_2) and the nonlinear absorption coefficient (β) were determined for different normality of $KMnO_4$ solution. Also, using the values of n_2 and β, the third-order nonlinear susceptibility (χ^3) was discovered. The normality *versus* nonlinear refractive index has been assessed by plotting a curve. The closed aperture response reveals the negative sign of the nonlinear refractive index, which indicates the self-defocusing behavior, and the open aperture response demonstrates the reverse saturable absorption (RSA) mechanism. The thermal nature of the $KMnO_4$ was found by the order of magnitude of the nonlinear refractive index (n_2) and also by investigating the peak-valley separation values. The studies led to further investigation in the field of optical switching.

1. Introduction

Nonlinear optics (NLO) is concerned with how the electromagnetic field of a light wave interacts with the electromagnetic fields of matter and of other light waves. The interaction of light with a nonlinear optical material will cause the material's properties to change. These interactions may change the frequency, phase, polarization, or path of incident light.[1] In the Z-scan experiment, refraction and multi photon absorption, a process through which multiple photons are absorbed by molecules or materials for electronic transitions, are the dominant interaction mechanisms. The Z-scan method has gained rapid acceptance by the nonlinear optics community due to the simplicity of the technique as well as the simplicity of the interpretation, it can rapidly measure both nonlinear absorption (NLA) and nonlinear refraction (NLR) in solids, liquids, and liquid solutions.[2] The Z-scan is a single-beam technique for measuring the sign and magnitude of refractive nonlinearities. The technique is based on the transformation of phase distortion to amplitude distortion during beam propagation.[3] The phase distortion arises from an optically induced nonlinear self-phase modulation (SPM), when the laser beam propagates inside the sample. SPM changes the phase of an optical pulse resulting from the nonlinearity of the refractive index of the material medium.[4] One can simultaneously measure the sign and magnitude of the nonlinear refraction from the closed aperture (CA) response and nonlinear absorption from the open aperture (OA) response of the nonlinear materials, which are proportional to the real part Re $\chi^{(3)}$ and imaginary part Im $\chi^{(3)}$ of the third order nonlinear susceptibilities. Materials with high optical nonlinearities of second-order and superior third-order nonlinear response find applications in the field of optical limiting and in the fields of photonics, including information processing, data storage devices and optical switching. Z-scan has been used in oncology to discriminate between solid tumors and to identify tumor-circulating cell-free DNA in liquid samples.[5]

Exploration of potassium permanganate in the NLO region is of primary importance due to the specific molecular structural bonding. Since its discovery in 1659, potassium permanganate has a long history of application to different fields, such as catalysis, medicine and electrochemical and mechanical areas. The use of potassium permanganate in the synthesis area was achieved to prepare many manganese oxide nanostructures. Potassium permanganate exhibits a wealth of physical and chemical properties originating from the electronic states of Mn^{7+} ($3d^0$) tetrahedrally surrounded by four oxygen anions.[6]

Department of Physics, St. George's College, Aruvithura, Kottayam, Kerala – 686122, India. E-mail: skrsgc@gmail.com, eldoabrahamthomas@gmail.com, 10sandeepsuresh@gmail.com

The quantum theory of atoms in molecules was applied to characterize the topological parameters of $KMnO_4$ revealing that the K–O bond has pure ionic characteristics, while the Mn–O bonds show an intermediate behaviour of electron density.[7] The X-ray powder diffraction pattern of $KMnO_4$ presents the most intense peak at $2\theta = 24.08°$, and some other representative peaks at $2\theta = 15.58°$, 18.84°, 22.92°, 25.00°, 26.61°, 27.94°, 30.4°, 41.42°, 35.12°, 41.46°, 49.76°, 52.08° and 54.76°, being consistent with diffractograms reported for this material (JCPDS file 89-3951). In the FTIR spectrum of $KMnO_4$, the band at 902 cm^{-1} is assigned to the ν_3 mode of MnO_4 and the small bands at 1812 and 1734 cm^{-1} also correspond to specific vibrations of $KMnO_4$.[8] The thermal decomposition of $KMnO_4$ (described by TG-DTA studies) occurs at a noticeable rate at temperatures ranging from 200 to 280 °C. The chemical reaction can be described schematically as $2KMnO_4 \rightarrow K_2MnO_4 + MnO_2 + O_2$, the solid products being manganese dioxide and potassium manganate, and the gaseous product oxygen.[9] The novelty of this study lies in the selection of this material in the context of its industrial as well as scientific application along with exploring the hidden optical properties especially in the nonlinear domain, which gives an insight into the physicochemical properties, and enables a better exploitation of the material. This study investigates the third-order nonlinear optical properties of pure $KMnO_4$ using the continuous wave Z-scan technique, a method not anywhere previously applied to this material.

2. Preparation of the sample

Potassium permanganate is an inorganic compound represented using the chemical formula $KMnO_4$. It is a purplish-black crystalline salt that dissolves in water to give an intense pink to purple color solution. It dissolves in water as K^+ and MnO_4^- as shown in Fig. 1. Potassium permanganate belongs to the orthorhombic space group *Pnma* 062, with cell dimensions a = 9.09 Å, b = 7.41 Å, c = 5.72 Å, with four molecules per unit cell.[10] It has a molar mass of 158.034 g mol^{-1} and the molality of $KMnO_4$ is 1.58 g mL^{-1}.

Using a high-precision common balance, 1.6 g of $KMnO_4$ was weighed and then dissolved into a beaker containing 500 mL of distilled water. The solution was stirred for 15 minutes using a magnetic stirrer to ensure that the crystals were completely dissolved.

Using the normality equation, $N_1V_1 = N_2V_2$, an adequate amount of double distilled water (ddH_2O) was added to prepare $KMnO_4$ solutions with normalities of 0.05 N (sample 1), 0.0166 N (sample 2), 0.0125 N (sample 3), and 0.009 N (sample 4). The $KMnO_4$ solution of normality 0.05 N has an intense purple colour, and as the normality decreases, the transparency of the sample increases giving different shades of purple colour.

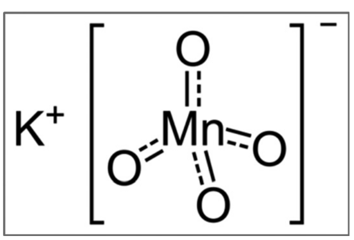

Fig. 1 Structure of potassium permanganate ($KMnO_4$).

The prepared $KMnO_4$ samples were then filled into the cuvette, having a path length of 1 mm and a volume of 0.35 mL. The cuvette is then placed on the translational stage for scanning.

3. Characterization techniques

3.1 UV-visible spectroscopy

A UV1700 Pharmaspec Shimadzu UV-vis spectrophotometer was used for the spectral analysis of the specimens. Ultraviolet-visible spectroscopy is a technique used to perform both qualitative and quantitative analyses of a specimen using a light source at the ultraviolet wavelength range of 200–400 nm to the visible wavelength range of 400–700 nm. The interaction between the light source and specimen can be analyzed through the absorption, transmission, or reflection in the UV-Vis spectrum. The characteristics peak in the UV-Vis spectrum is a representation of the energy bonding of the specimen.[11] From the absorbance data of the UV-Vis spectrum, the absorption coefficient can be evaluated using the relation,

$$\alpha = 2.303\left(\frac{A}{t}\right) \quad (1)$$

where A represents the absorbance of the specimen as indicated by the spectrum at the desired wavelength and t represents the thickness of the specimen along which the light source propagates.

3.2. Z-scan technique

The Z-scan experimental arrangement is illustrated in Fig. 2. The Holmarc Z scan system model: HO-ED-LOE-03 was used for the experiment. The laser beam source used is a continuous wave (CW) diode pumped solid state (DPSS) laser (crystal) module producing an output of 532 nm, 100 mW of Gaussian nature. A lens with a focal length of 286 mm was used to focus the beam. The sample is then placed in the precision motorized stage for linear scanning. Upon scanning, the sample travels 150 mm in the linear translation stage from $-z$ to $+z$ with a minimum step size of 0.1 mm through the beam waist, at $z = 0$. The beam waist refers to the point where the beam is most constricted, representing a position linked to the smallest beam radius, denoted as w_0. The required scan range in an experiment depends on the beam parameters and the sample thickness L. One of the critical parameters is the Rayleigh length, Z_R, of the focused beam defined as $\pi w_0^2/\lambda$ for a Gaussian beam where w_0 is the focal spot size.

For "thin" samples (*i.e.* $L \leq Z_R$, sample thickness must be less than or equal to Rayleigh length), although all the information is theoretically contained within a scan range of $\pm Z_R$, it is preferable to scan the sample for $\approx \pm 5Z_R$ or more. This requirement, as we shall see, simplifies data interpretation when the sample's surface roughness or optical beam imperfections

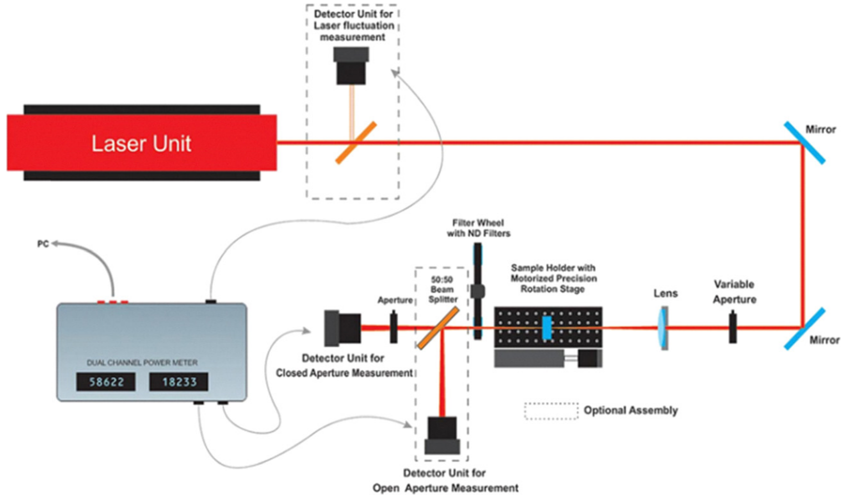

Fig. 2 Z-scan experimental setup.

introduce background "noise" into the measurement system.[2] We measure the transmittance through the aperture placed at the far field *i.e.* $+z_\infty$ on a detector for closed aperture Z-scan and without aperture for open aperture Z-scan. The position of the aperture is rather arbitrary as long as its distance from the focus, $d \gg Z_R$. Typical value ranges are from $20Z_R$ to $100Z_R^2$. A real-time plot of transmitted power (μW) *versus* position (mm) is obtained along with the data in the Z-scan system software. The axes of the real-time plot are then normalized to give normalized transmittance on the *y*-axis and position on the *x*-axis. Theoretical response for Z-scan closed aperture (CA) and open aperture (OA) is shown in Fig. 3 and 4 respectively.

In the context of CA response, the graph depicted in Fig. 3 illustrates that a pre-focal transmittance maximum (peak) followed by a post-focal transmittance minimum (valley) is, therefore, the Z-scan signature of a negative refractive nonlinearity,[12] and conversely for positive nonlinear refraction. As the sample traverses the Rayleigh length, it exhibits characteristics akin to a concave lens, causing the Gaussian beam to self-defocus and resulting in a peak-valley response. Conversely, the sample behaves like a convex lens, autonomously focusing the Gaussian beam and yielding a valley-peak response. The difference in the ordinate values of the maximum and the minimum, ΔT_{pv} (*i.e.* the peak-to-valley height),

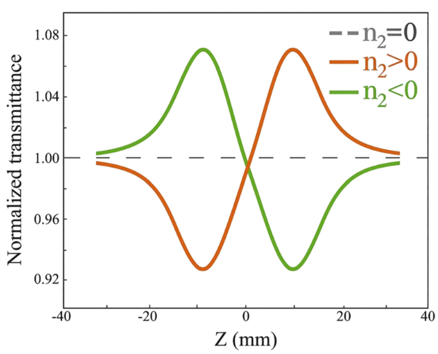

Fig. 3 Theoretical response of a closed aperture Z-scan.

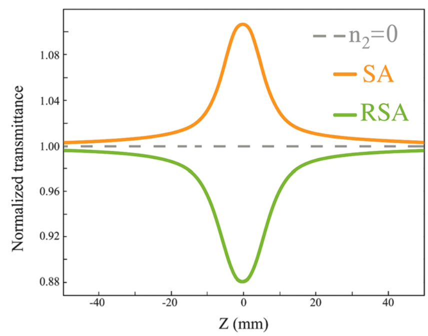

Fig. 4 Theoretical response of an open aperture Z-scan.

is an indirect measure of the amount of nonlinear refraction.[13] Several diverse physical effects contribute to the nonlinear index of refraction. Generally, it can be defined as a change in the refractive index or the spatial distribution of the refractive index of a medium due to the presence of optical waves. Several different types of effects fall under this general definition, namely the optical Kerr effect, nonlocal effects, saturation, changes in physical properties of a medium, and cascading effects.[14] The on-axial nonlinear phase shift induced by the sample is

$$|\Delta\varphi| = \frac{\Delta T_{pv}}{0.406(1-S)^{0.25}} \tag{2}$$

where $S = 1 - \exp(-2r_a^2/W_a^2)$, the linear transmittance of the aperture in the absence of the sample, r_a is the aperture radius and W_a is the beam radius at the aperture. In most reported experiments, $0.1 < S < 0.5$ has been used for determining nonlinear refraction.[2] The nonlinear refractive index n_2 can be obtained using the relation

$$n_2 = \frac{|\Delta\varphi|\lambda}{2\pi I_0 L_{eff}}\ \mathrm{m^2\ W^{-1}} \tag{3}$$

where $I_0 = 2P_0/\pi w_0^2$ represents the axial irradiance at the beam waist, $L_{eff} = (1 - \exp(-\alpha L))/\alpha$ represents the effective sample length, α is the absorption coefficient and L denotes the sample thickness.

The open aperture Z-scan trace corresponds to the absorption of the material as shown in Fig. 4. Nonlinear absorption will only happen when the sample is subject to a high-intensity laser beam. Consider a system with two energy levels, say E_1 being the ground energy level and E_2 being the excited level. N_1 and n_2 are the populations of the atoms/molecules in the ground and excited energy levels, respectively. The lower-level atoms/molecules can absorb a photon of frequency υ and energy $E = h\nu = (E_2 - E_1)$. However, suppose the number of photons incident simultaneously on this system is just equal to the number of atoms/molecules in the lower energy state, the entire absorbing atoms/molecules could be excited to the higher level at unity quantum yield, making the lower level momentarily empty. If one more photon of the same energy is incident after this, there is no more atom/molecule to absorb this and hence the photon passes through, leading to a case of ’induced transparency’. Thus, the material that was opaque to a smaller number of photons has now become transparent when a large number of photons are incident. This is called saturable absorption (SA). Another interesting possibility for an atom excited to the first excited state by the incident laser beam is that there could be transitions to further higher states, in the case of a multi-level system with appropriate energy levels. Thus, the upper level can be momentarily depleted, leading to further absorption and a corresponding decrease in transition. This is known as reverse saturable absorption (RSA).[13] The nonlinear absorption coefficient β associated with the open aperture Z-scan technique can be determined by employing the relation,

$$\beta = \frac{2\sqrt{2}\Delta T}{I_0 L_{\mathrm{eff}}}\ \mathrm{m\ W^{-1}} \tag{4}$$

The value of ΔT can be directly determined from the normalized open aperture response. The real and imaginary parts of the third-order nonlinear susceptibility can be derived from the nonlinear index of refraction and the coefficient of nonlinear absorption.

$$\mathrm{Re}\,\chi^{(3)} = 2cn_2\varepsilon_0{n_0}^2\ \mathrm{m^2\ V^{-2}} \tag{5}$$

$$\mathrm{Im}\,\chi^{(3)} = \frac{c\lambda\beta\varepsilon_0{n_0}^2}{3\pi}\ \mathrm{m^2\ V^{-2}} \tag{6}$$

where ε_0 represents the permittivity of free space, c is the velocity of light, and n_0 denotes the linear refractive index of the sample. The magnitude of the third-order nonlinear susceptibility $\chi^{(3)}$ can be approximated using

$$\chi^{(3)} = \sqrt{\left(\mathrm{Re}\,\chi^{(3)}\right)^2 + \left(\mathrm{Im}\,\chi^{(3)}\right)^2}\ \mathrm{m^2\ V^{-2}} \tag{7}$$

4. Results and discussion

4.1. UV-vis spectrum

Fig. 5 shows the ultraviolet-visible spectrum of the $KMnO_4$ sample of normalities of 0.05 N, 0.0166 N, 0.0125 N, and 0.009 N, which are indicated using black, red, blue, and purple lines, respectively. The spectrum yields the following information. $KMnO_4$ with normality 0.05 N shows near saturation or saturation at all wavelengths. Also, 0.0125 N normal $KMnO_4$ solution shows minimal absorbance at all wavelengths from 200 nm to 700 nm. While observing from the lower wavelength side of the UV-Vis spectrum, it is found that the samples with increasing normality de-excite first from the saturation levels for wavelengths ranging from 243 nm to 387 nm. Also, the samples show excitation in the reverse order as they de-excite. At 537 nm, it is found that all samples with different normality will de-excite and rapidly decay into nominal absorbance. From 200 nm to 242 nm, 293 nm to 364 nm, and 506 nm to 532 nm all the samples with different normality show the maximum absorbance. According to the spectrum, the absorbance value at a wavelength of 532 nm was consistently 4 for all normalities of $KMnO_4$. By employing eqn (1), the linear absorption coefficient, α, is calculated to be 0.9212 $\mathrm{mm^{-1}}$. Here, materials exhibiting high optical transparency (as indicated by UV-vis data) are expected to correlate with better NLO performance.

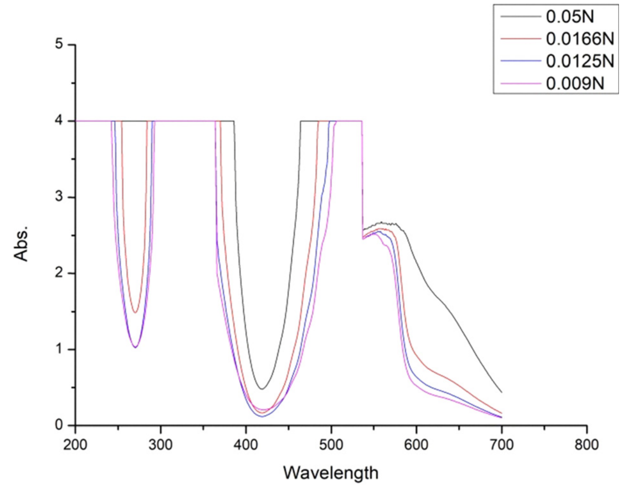

Fig. 5 UV-vis spectrum of $KMnO_4$ solutions of 0.05 N, 0.0166 N, 0.0125 N and 0.009 N.

4.2 Sample 1-$KMnO_4$ of normality 0.05 N

Fig. 6 illustrates the closed aperture response, which indicates a negative sign for the nonlinear refractive index, whereas Fig. 7 reveals the reverse saturable absorption (RSA) mechanism in the open aperture response. The normalized transmittance, denoted as $T(z)$, can be derived from the relation:

$$T(z) = \frac{P(z)}{P(\infty)},$$

where, $P(z)$ is the power at the z position and $P(\infty)$ is taken as the power at a position far from focus. The beam waist, w_0, to which the sample is symmetrically translated, can be calculated using the equation, $w_0 = 2f\lambda/D\pi$. Here, f is the focal length (28.6 cm) of the lens placed before the translational stage, λ is the laser wavelength, and D is the diameter of the beam entering the lens. The calculated beam waist (w_0) is 24 μm.

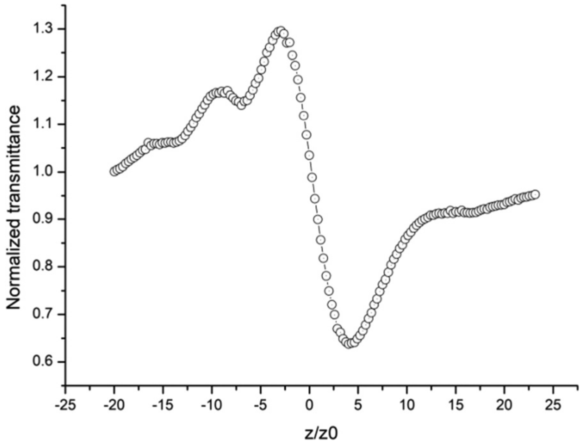

Fig. 6 Normalized closed aperture response of 0.05 N $KMnO_4$.

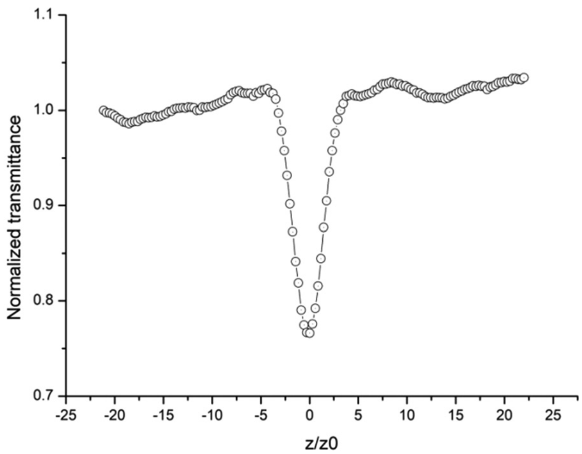

Fig. 7 Normalized open aperture response of 0.05 N $KMnO_4$.

The peak-valley separation ΔT_{pv} can be obtained explicitly from Fig. 8. The on-axis phase shift is evaluated using eqn (2),

$$|\Delta\varphi| = \frac{\Delta T_{pv}}{0.406(1-S)^{0.25}},$$

where $S \sim 0.25$.

The third order nonlinear refractive index n_2 was calculated to be 2.071×10^{-12} m^2 W^{-1} using eqn (3),

$n_2 = \frac{|\Delta\varphi|}{kI_0L_{eff}}$ where I_0 is the peak irradiance at the beam waist and is estimated to be 108.760 MW m^{-2}. Also, the magnitude of the nonlinear absorption corresponding to the reverse saturable absorption mechanism was explored by employing the relation specified in eqn (4),

$$\beta = \frac{2\sqrt{2}\Delta T}{I_0 L_{eff}}$$

is calculated to be 1.069×10^{-5} m W^{-1}. These values are then utilized in the computation of complex equations encompassing both the real and imaginary components of the third-order nonlinear optical susceptibility $\chi^{(3)}$

$$\mathrm{Re}\,\chi^{(3)} = 2cn_2\varepsilon_0 n_0^{\,2}\ \mathrm{m^2\ V^{-2}}$$

$$\mathrm{Im}\,\chi^{(3)} = \frac{c\lambda\beta\varepsilon_0 n_0^{\,2}}{3\pi}\ \mathrm{m^2\ V^{-2}}$$

The real and imaginary parts of the third-order nonlinear optical susceptibility were determined to be 2.781×10^{-14} m^2 V^{-2} and 4.056×10^{-15} m^2 V^{-2}, respectively. The magnitude of the third-order nonlinear susceptibility $\chi^{(3)}$ can be approximated using

$$\chi^{(3)} = \sqrt{\left(\mathrm{Re}\,\chi^{(3)}\right)^2 + \left(\mathrm{Im}\,\chi^{(3)}\right)^2}\ \mathrm{m^2\ V^{-2}}$$

and was estimated to be 2.811×10^{-14} m^2 V^{-2}. The figure of merit factors W and T were obtained using the nonlinear refractive index and absorption coefficient through the relations

$$W = \frac{n_2 I_0}{\lambda\alpha_0}\ \text{and}\ T = \frac{\beta\lambda}{n_2}.$$

For all-optical switching applications, the figure of merit W should be greater than one and T should be less than one.[15] However, here the merit factors were evaluated to be 0.459 and 2.747 for W and T, respectively.

4.3. Sample 2-$KMnO_4$ of normality 0.0166 N

Fig. 8 and 9 depict the closed aperture and open aperture response when $KMnO_4$ of 0.0166 N was subject to a high-intensity beam. It is evident from the above Fig. 8 that, for the particular normality of $KMnO_4$, the sample acts as a concave lens resulting in a negative nonlinear refractive index n_2. Also, Fig. 9 confirms that the sample has a multi-level energy system, thus yielding a typical reverse saturable absorption (RSA) response. The values of nonlinear refractive index, n_2, and the nonlinear absorption coefficient, β, were calculated as above and found to be 2.728×10^{-12} m^2 W^{-1} and 1.663×10^{-5} m W^{-1}, respectively. The quantities such as $\mathrm{Re}\,\chi^{(3)}$ and $\mathrm{Im}\,\chi^{(3)}$ were calculated to be 3.664×10^{-14} m^2 V^{-2} and 6.308×10^{-15} m^2 V^{-2}, thus making the total third-order susceptibility $\chi^{(3)}$ as

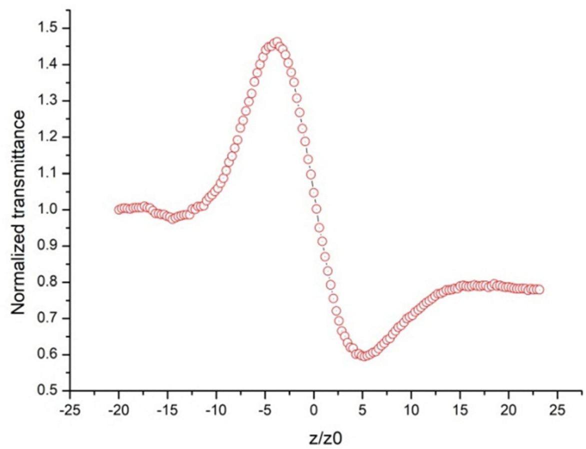

Fig. 8 Normalized closed aperture response of 0.0166 N $KMnO_4$.

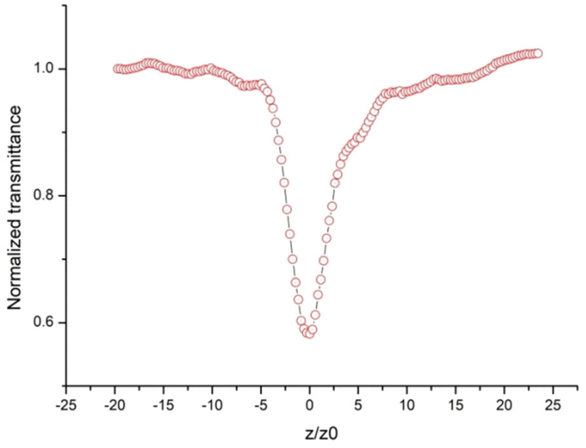

Fig. 9 Normalized open aperture response of 0.0166 N $KMnO_4$.

3.718×10^{-14} m^2 V^{-2}. The figure of merit factors W and T were estimated to be 0.605 and 3.243, respectively.

4.4. Sample 3-$KMnO_4$ of normality 0.0125 N

Fig. 10 illustrates the closed aperture response of sample 3. The pre-focal transmittance peak followed by a post-focal transmittance valley is the ideal character of negative refractive nonlinearity. From this figure, we can directly assess the peak-valley separation ΔT_{pv} as 0.670, enabling us to determine the on-axis phase shift, $|\Delta\varphi|$ as 1.771, using the aforementioned relation in 4.2. By utilizing the relation for the nonlinear refractive index mentioned in eqn (3), we obtain n_2 as 2.111×10^{-12} m^2 W^{-1}. The real part of the third-order nonlinear susceptibility, which is proportional to the refractive nonlinearity by the relation mentioned in eqn (5), is obtained as 2.835×10^{-14} m^2 V^{-2}. The figure of merit factor W was found to be 0.468.

4.5. Sample 4-$KMnO_4$ of normality 0.009 N

A negative sign for the refractive nonlinearity is well depicted in the normalized closed aperture response of sample 4 in Fig. 11. Such a response corresponds to the self-defocusing character of the sample. ΔT_{pv} can be explicitly found from the peak-valley graph, which is then used to find the axial phase shift $|\Delta\varphi|$. The real part of susceptibility $\mathrm{Re}\,\chi^{(3)}$ was found to be 2.167×10^{-14} m^2 V^{-2}, using the third-order nonlinear refractive index 1.614×10^{-12} m^2 W^{-1}. The coefficient of the figure of merit factor W was estimated to be 0.358. Comparing $KMnO_4$ of normality 0.009 N with other normality reveals that sample 4 has the lowest values for all nonlinear optical parameters.

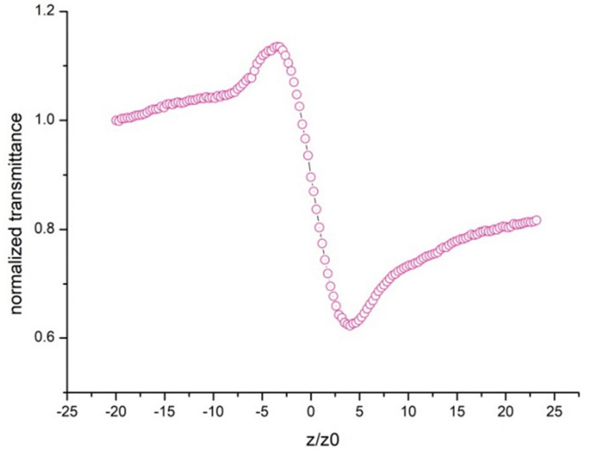

Fig. 11 Normalized closed aperture response of 0.009 N $KMnO_4$.

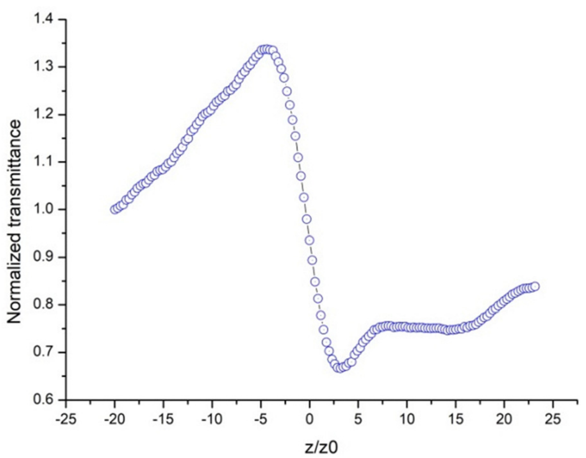

Fig. 10 Normalized closed aperture response of 0.0125 N $KMnO_4$.

For concise presentation, the numerical data from the study can be effectively summarised through the integration of tabular columns and figures. A comparison between the nonlinear optical parameters from the closed and the open aperture Z-scan technique is tabulated as Table 1. It is explicit that the NLO behaviour of pure $KMnO_4$ is superior to several other reported inorganic samples.[16]

It's clear from Fig. 12 that the nonlinear refraction demonstrates an almost steady increase with the rising normality of the $KMnO_4$ solution. It led to the fact that the number of molecules participating increases as the normality of the $KMnO_4$ solution increases, and a greater number of particles are thermally agitated leading to an amplified optical nonlinearity.

5. Conclusion

The pure $KMnO_4$ crystals were dissolved in ddH_2O to obtain a $KMnO_4$ solution of normality 0.05 N, 0.0166 N, 0.0125 N, and 0.009 N. The third-order nonlinear optical properties such as nonlinear refractive index (n_2), nonlinear absorption (β), and third-order nonlinear susceptibility ($\chi^{(3)}$) were studied using the Z-scan characterization technique. The results from the study yield that the $KMnO_4$ solution has a negative nonlinear refractive index since the sample acts as a concave lens resulting in the self-defocusing of the incident beam in the closed aperture Z-scan technique. The magnitude of the nonlinear refractive index (n_2) was found to be of the order of 10^{-12} m^2 W^{-1}, which corresponds to the thermal contributions of the sample.[14] Also, in the materials that show thermal-type optical nonlinearities, the peak-valley separation values are greater than $1.7Z_R{}^4$. The

Table 1 Comparison of closed and open aperture parameters

N	$\|\Delta\varphi\|$	n_2 ($m^2\ W^{-1}$)	Re $\chi^{(3)}$ ($m^2\ V^{-2}$)	β ($m\ W^{-1}$)	Im $\chi^{(3)}$ ($m^2\ V^{-2}$)	$\chi^{(3)}$ ($m^2\ V^{-2}$)	W	T
0.05	1.737	2.071×10^{-12}	2.781×10^{-14}	1.069×10^{-5}	4.056×10^{-15}	2.811×10^{-14}	0.459	2.747
0.0166	2.289	2.728×10^{-12}	3.664×10^{-14}	1.663×10^{-5}	6.308×10^{-15}	3.718×10^{-14}	0.605	3.243

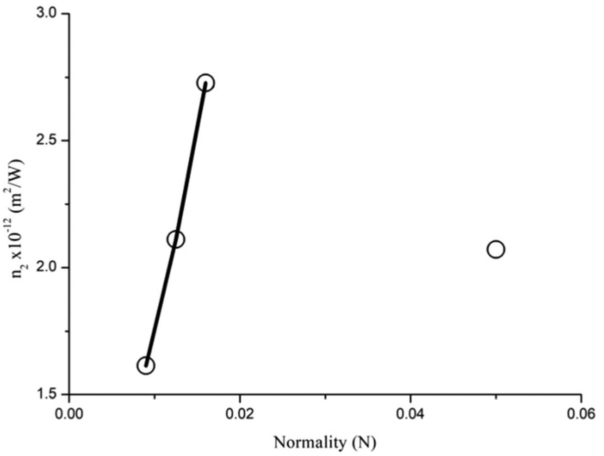

Fig. 12 Normality dependence of n_2 for $KMnO_4$.

Table 2 Closed aperture parameters of all normalities of $KMnO_4$

N	ΔZ_{pv} (mm)	ΔT_{pv}	$\|\Delta\varphi\|$	n_2 ($m^2\ W^{-1}$)	Re $\chi^{(3)}$ ($m^2\ V^{-2}$)	W
0.05	6.94	0.658	1.737	2.071×10^{-12}	2.781×10^{-14}	0.459
0.0166	8.92	0.867	2.289	2.728×10^{-12}	3.664×10^{-14}	0.605
0.0125	7.52	0.670	1.771	2.111×10^{-12}	2.835×10^{-14}	0.468
0.009	7.52	0.512	1.354	1.614×10^{-12}	2.167×10^{-14}	0.358

average peak-valley separation (ΔZ_{pv}), from Table 2, exhibited by the closed aperture Z-scan response of $KMnO_4$ is $2.2Z_R$, which again validates the thermal nature of the specimens. It was also confirmed that the samples possess nonlinear absorption characteristics. From the open aperture Z-scan responses it is evident that the molecules make transitions into the higher energy levels by absorbing photons from the incident laser beam, thus confirming that the sample has a multi-level system with appropriate energy levels. It is thus concluded that the $KMnO_4$ has reverse saturable absorption (RSA). The study also reveals a general trend, depicted in Table 2, among the samples that normality is related to the third-order nonlinear optical parameters such as refraction, absorption, and susceptibility. The results from the figure of merit factors indicate a poor application in the field of optical switching. But, the development of advanced complex composite films by tuning the bandgap energy, absorption properties, and electrical conductivity has attracted attention because of their application in advanced optoelectronic devices.

Declaration of generative AI and AI-assisted technologies in the writing process

During the preparation of this work the authors used ChatGPT 3.5 in order to improve readability and language. After using this tool, the authors reviewed and edited the content as needed and take full responsibility for the content of the publication.

Conflicts of interest

The authors declare that they have no known competing financial interests or personal relationships that could have appeared to influence the work reported in this paper.

Data availability

The authors declare that the data supporting the findings of this study are available within the paper and its supplementary information (SI). Supplementary information is available. See DOI: **https://doi.org/10.1039/d5ma00947b**.

Acknowledgements

This research did not receive any specific grant from funding agencies in the public, commercial, or not-for-profit sectors. Author Santhosh Kumar R acknowledges the Department of Science & Technology for their funding through the DST-FIST scheme to purchase the Z-scan system. We deeply acknowledge the technical support provided by the Holmarc Opto-Mechatronics Ltd engineer Mr Lageesh Madhu and Mr Kiran John U, Department of Physics, Sacred Heart College, Thevara for providing conceptual support during our work.

References

1 G. D. Stucky, S. R. Marder and J. E. Sohn, *Linear and Nonlinear Polarizability. in Materials for Nonlinear Optics*, American Chemical Society, 1991, vol. 455, pp. 2–30, DOI: **10.1021/bk-1991-0455.ch001**.
2 E. W. Van Stryland and M. Sheik-Bahae *Z-Scan Measurements of Optical Nonlinearities*, (2004), DOI: **10.1201/9781315139036**.
3 M. Sheik-Bahae, A. A. Said and E. W. Van Stryland, High-sensitivity, single-beam n_2 measurements, *Opt. Lett.*, 1989, **14**, 955–957, DOI: **10.1364/OL.14.000955**.
4 S. Jeyaram and T. Geethakrishnan, Third-order nonlinear optical properties of acid green 25 dye by Z-scan method, *Opt. Laser Technol.*, 2017, **89**, 179–185, DOI: **10.1016/j.optlastec.2016.10.006**.
5 F. L. A. Fonseca, G. L. da Veiga, B. da Costa Aguiar Alves and S. I. P. M. do Nascimento Alves, Liquid biopsy in cancer using the Z-scan technique: a new approach to discover biomarkers in cancer, *Future Sci. OA*, 2020, **7**, FSO638, DOI: **10.2144/fsoa-2020-0054**.

6 K. A. M. Ahmed, Exploitation of $KMnO_4$ material as precursors for the fabrication of manganese oxide nanomaterials, *J. Taibah Univ. Sci.*, 2016, **10**(3), 412–429, DOI: 10.1016/j.jtusci.2015.06.005.

7 D. Marabello, R. Bianchi, G. Gervasio and F. Cargnoni, An experimental (120 K) and theoretical electron-density study of $KMnO_4$ and $KClO_4$, *Acta Cryst. A*, 2004, **60**, 494–501, DOI: 10.1107/S0108767304015260.

8 M. E. Becerra, N. P. Arias, O. H. Giraldo, F. E. López Suárez, M. J. Illán Gómez and A. Bueno López, Soot combustion manganese catalysts prepared by thermal decomposition of KMnO4, *Appl. Catal., B*, 2011, **102**, 1–2, DOI: 10.1016/j.apcatb.2010.12.006.

9 J. S. Booth, D. Dollimore and G. R. Heal, Thermal analysis of some group I permanganate decompositions, *Thermochim. Acta*, 1980, **39**(3), 281–291, DOI: 10.1016/0040-6031(80)87080-8.

10 S. Ramaseshan, K. Venkatesan and N. V. Mani, The use of anomalous scattering for the determination of crystal structures-$KMnO_4$, *Proc. Ind. Acad Sci. – Sect. A*, 1957, **46**, 95–111, DOI: 10.1007/BF03045960.

11 K. Thambiratnam, S. A. Reduan, Z. C. Tiu and H. Ahmad, in Chapter 9 – Application of two-dimensional materials in fiber laser systems, *Nano-Optics*, ed. Thomas, S., Grohens, Y., Vignaud, G., Kalarikkal, N. & James, J., Elsevier, 2020, pp. 227–264, DOI: 10.1016/B978-0-12-818392-2.00009-3.

12 M. Sheik-Bahae, A. A. Said, T. H. Wei, D. J. Hagan and E. Ws Van Stryland, Sensitive measurement of optical nonlinearities using a single beam, *IEEE J. Quantum Electron.*, 1990, **26**, 760–769, DOI: 10.1109/3.53394.

13 Y. Murti and C. Vijayan, Self Focusing, Phase Modulation and Pulse Shaping, *Essentials of Nonlinear Optics*, 2014, 125–145, DOI: 10.1002/9781118902332.ch7.

14 R. L. Sutherland, D. G. McLean and S. Kirkpatrick, *Handbook of Nonlinear Optics*, Marcel Dekker, 2003, DOI: 10.1201/9780203912539.

15 U. K. John and S. Mathew, Z-scan investigations on the third order nonlinear optical properties of flower-like CdZnTe microstructures, *Appl. Phys. A*, 2022, **128**, 259, DOI: 10.1007/s00339-022-05395-2.

16 N. Priyadarshani, G. Vinitha and T. C. S. Girisun, Third order nonlinear optical properties of monoclinic and orthorhombic CuNb2O6 under CW laser illumination, *Opt. Laser Technol.*, 2018, **108**, 287–294, DOI: 10.1016/j.optlastec.2018.06.040.